NEURAL REGENERATION RESEARCH
February 2017, Volume 12, Issue 2
www.nrronline.org

RESEARCH ARTICLE

Delayed treatment of secondary degeneration following acute optic nerve transection using a combination of ion channel inhibitors

Nathanael J. Yates[1], Marcus K. Giacci[1], Ryan L. O'Hare Doig[1, 2], Wissam Chiha[1, 2], Bethany E. Ashworth[1], Jade Kenna[1], Carole A. Bartlett[1], Melinda Fitzgerald[1, *]

1 Department of Experimental and Regenerative Neurosciences, School of Animal Biology, The University of Western Australia, Crawley, Western Australia, Australia

2 Department of Experimental and Regenerative Neurosciences, School of Anatomy, Physiology and Human Biology, The University of Western Australia, Crawley, Western Australia, Australia

How to cite this article: *Yates NJ, Giacci MK, O'Hare Doig RL, Chiha W, Ashworth BE, Kenna J, Bartlett CA, Fitzgerald M (2017) Delayed treatment of secondary degeneration following acute optic nerve transection using a combination of ion channel inhibitors. Neural Regen Res 12(2):307-316.*

Open access statement: *This is an open access article distributed under the terms of the Creative Commons Attribution-NonCommercial-ShareAlike 3.0 License, which allows others to remix, tweak, and build upon the work non-commercially, as long as the author is credited and the new creations are licensed under the identical terms.*

Funding: *We acknowledged financial support from the National Health and Medical Research Council (NHMRC), Australia (APP1061791). MF was supported by an NHMRC Career Development Fellowship (APP1087114).*

Abstract

Studies have shown that a combined application of several ion channel inhibitors immediately after central nervous system injury can inhibit secondary degeneration. However, for clinical use, it is necessary to determine how long after injury the combined treatment of several ion channel inhibitors can be delayed and efficacy maintained. In this study, we delivered Ca^{2+} entry-inhibiting P2X7 receptor antagonist oxidized-ATP and AMPA receptor antagonist YM872 to the optic nerve injury site *via* an iPRECIO® pump immediately, 6 hours, 24 hours and 7 days after partial optic nerve transection surgery. In addition, all of the ion channel inhibitor treated rats were administered with calcium channel antagonist lomerizine hydrochloride. It is important to note that as a result of implantation of the particular pumps required for programmable delivery of therapeutics directly to the injury site, seromas occurred in a significant proportion of animals, indicating infection around the pumps in these animals. Improvements in visual function were observed only when treatment was delayed by 6 hours; phosphorylated Tau was reduced when treatment was delayed by 24 hours or 7 days. Improvements in structure of node/paranode of Ranvier and reductions in oxidative stress indicators were also only observed when treatment was delayed for 6 hours, 24 hours, or 7 days. Benefits of ion channel inhibitors were only observed with time-delayed treatment, suggesting that delayed therapy of Ca^{2+} ion channel inhibitors produces better neuroprotective effects on secondary degeneration, at least in the presence of seromas.

Key Words: *nerve regeneration; optic nerve injury; neurotrauma; secondary degeneration; seromas; calcium channel inhibitor; node of Ranvier; Tau phosphorylation; lipid peroxidation; oxidative stress; neural regeneration*

***Correspondence to:**
Melinda Fitzgerald, Ph.D., lindy.fitzgerald@uwa.edu.au.

orcid:
0000-0002-4823-8179 (Melinda Fitzgerald)

doi: *10.4103/1673-5374.200814*

Accepted: *2017-02-03*

Introduction

Following injury to the central nervous system, secondary degeneration of tissue surrounding the primary injury leads to further loss of cells and function. In these vulnerable regions, excitotoxicity and increased intracellular calcium (Ca^{2+}) contribute to mitochondrial dysfunction and oxidative stress (Park et al., 2004; Camello-Almaraz et al., 2006; Peng and Jou, 2010; O'Hare Doig et al., 2014).

Ca^{2+} entry pathways into neurons and glia involve voltage-gated Ca^{2+} channels, glutamate-activated N-methyl-D-aspartate receptors, α-amino-3-hydroxy-5-methyl-4-isoxazolepropionic acid receptors (AMPAR), and adenosine triphosphate activated purinergic P2X7 receptors (Agrawal et al., 2000; Matute et al., 2007; Hamilton et al., 2008). Inhibition of these receptors reduces Ca^{2+} entry (Akaike et al., 1993; Hamilton et al., 2008) as well as microglial activation, neuronal cell death, oxidative stress, and abnormalities in node/paranode structure (Yoles et al., 1997; Fitzgerald et al., 2009b; Selt et al., 2010; Savigni et al., 2013). In the partial optic nerve transection model of secondary degeneration, inhibition of multiple pathways of Ca^{2+} entry using combinations of ion channel inhibitors reduces chronic damage more effectively than targeting individual ion channels (Savigni et al., 2013). However, it is unknown how long after injury initiation of treatment can be delayed and efficacy maintained, making clinical translation of this therapeutic strategy problematic.

Infection is a confounding factor frequently occurring in severe neurotrauma (O'Connor et al., 2004) and/or subsequent surgical interventions (Korinek, 1997). However, the effects of infection on secondary degeneration and efficacy of therapeutic agents are largely unknown. Here, we examine the

therapeutic window of the combinatorial ion channel inhibitor treatment using the partial optic nerve transection model of secondary degeneration, where some animals experienced seromas surrounding the drug delivery pump implantation site.

Materials and Methods

Animals

All experiments were approved by The University of Western Australia animal ethics committee (Approval number RA03/100/673) and were performed in accordance with National Institutes of Health guide for the care and use of Laboratory animals (NIH Publications No. 8023, revised 1978). Adult female Piebald Virol Glaxo (PVG) rats were supplied by the Animal Resource Centre (Murdoch, Western Australia). PVG rats were used as they are non-albino, facilitating assessments of visual function, and in order to build upon substantial characterization of secondary degeneration in this strain by our group (O'Hare Doig and Fitzgerald, 2015). Animals were provided with food and water *ad libitum* under 12 hour light/dark conditions and group-housed until surgery after which they were housed individually.

There were seven experimental groups with 6–12 animals per group (total n = 72, **Table 1**). The normal group received no surgery; the sham operated group (sham) received the surgical preparation for the partial optic nerve transection (PT) surgery and iPRECIO® pump implantation with immediate delivery of vehicle, but the dura surrounding the optic nerve was not cut and PT was not performed (surgical procedures described below). The five PT groups received PT and pump implantation, with immediate delivery of vehicle (PT-Veh) or the Ca^{2+} channel inhibitors (PT-t0) (described below): or delayed delivery, with Ca^{2+} channel inhibitor treatment initiated at 6 hours (PT-t6), 24 hours (PT-t24) or 7 days (PT-td7).

Surgery and treatments

PT was performed as described previously (Levkovitch-Verbin et al., 2003; Fitzgerald et al., 2009b). Briefly, rats were anesthetized with ketamine and xylazine intraperitoneally (ketamine hydrochloride, 50 mg/kg and xylazil hydrochloride, 10 mg/kg, Troy Laboratories, Glendenning, Australia). The right optic nerve was exposed approximately 1 mm behind the eye *via* a cut in the dura. The PT was delivered as a 200 μm cut on the dorsal aspect of the nerve using a diamond radial keratotomy knife (Geuder AG, Heidelberg, Germany). Sterile conditions were maintained throughout all surgical procedures in accordance with normal veterinary standards, including triple swabbing of surgical sites with povidone-iodine solution and 70% ethanol, and autoclave sterilization of all instruments.

All animals receiving PT and the sham operation were also implanted with a micro infusion programmable pump (model: MK02_V2, iPRECIO®) to deliver ion channel inhibitors or vehicle to the site of injury, based upon a modification of our previous protocol (Savigni et al., 2013). The programmable iPRECIO® pumps allow commencement of inhibitor delivery at a defined time, and were used in preference to Alzet osmotic mini-pumps for this study of therapeutic window. Immediately prior to the surgery, the pumps were filled with sterile phosphate buffered saline (PBS) vehicle or the ion channel inhibitors 1 mM oxidised-ATP (oxATP; Sigma, Sydney, New South Wales, Australia) and 240 μM Zonampanel (YM872, LKT Laboratories, St. Paul, MN, USA) in sterile PBS, and programmed for immediate or delayed-release schedules with delivery at 1 μL/h until the end of experiment. Sterility of the pumps was carefully maintained prior to implantation. At the time of PT surgery and immediately prior to PT, the pump was inserted into a subcutaneous pocket on the right flank and the catheter fed under the skin to the orbit where it was secured in place using superglue to attach the catheter to exposed bone. Following PT, the catheter from the pump was trimmed, so that the tip was close to the injury site immediately adjacent to the optic nerve. The surgery sites were closed using 6/0 Silk ram sutures. Povidone-iodine solution was applied to the wounds followed by subcutaneous analgesic (Norocarp, 2.8 mg/kg) and sterile PBS for rehydration. Animals recovered on a warming blanket until conscious, and were regularly monitored twice per day, 6 days per week until study completion.

In addition, all of the ion channel inhibitor treated groups (PT-t0 to PT-td7) were administered with lomerizine hydrochloride (30 mg/kg) orally in butter vehicle twice per day, at least 8 hours apart, commencing on the day of surgery immediately upon recovery from anaesthetic (PT-t0), or following a delay of 6 hours (PT-t6), 24 hours (PT-t24) or 7 days (PT-td7). Untreated groups (normal, sham, and PT-Veh) received the butter vehicle orally, commencing on the day of surgery (t0). Delayed treatment groups received the butter vehicle orally until lomerizine hydrochloride treatment commenced. Lomerizine dosage was based upon previous dose-response studies, established stability in butter, and previous treatment efficacy by this method of delivery (Karim et al., 2006; Fitzgerald et al., 2009b).

Optokinetic nystagmus

Two weeks post-surgery, all rats were anesthetised as above, and their left eyelids sutured shut (6/0 Silkram) to occlude vision in the uninjured left eye. On the following day, the animals were acclimatized to the testing room and tested for optokinetic nystagmus as a sensitive behavioural test of visual function (Abdeljalil et al., 2005). Briefly, animals were placed in the centre of a platform surrounded by a series of vertical black and white stripes of 5 mm thickness (0.13 cycles per degree, well within the 1.0–1.5 cycles per degree limits of visual acuity in pigmented rats measured binocularly (Prusky et al., 2002)) rotating around the stationary platform. After acclimatization, the head tracking movements in response to anticlockwise movement of the stripes were recorded for a 2-minute period. Analysis of the total number of head tracking movements, and the fast resetting of head location was performed blinded to experimental group. Results were corrected for the time each individual animal was engaged in the task.

Euthanasia and tissue preparation

On the day of testing for optokinetic nystagmus responses *i.e.*, 2 weeks after injury, rats were euthanized with Lethabarb (Sodium Pentobarbital, 850 mg/kg, i.p.), and transcardially perfused with 0.9% NaCl followed by 4% paraformaldehyde (VWR Chemicals) in phosphate buffer (0.1 M, pH 7.2). Right optic nerves were removed, and post-fixed overnight followed by cryoprotection in 15% sucrose in PBS. For immunohistochemical studies, tissue was frozen in optimal cutting temperature compound (Tissue-Tek® O.C.T. Compound, Sakura® Finetek, Tokyo, Japan) and a cryostat (CM1900, Leica, Mt Waverly, Victoria, Australia) was used to cut longitudinal optic nerve sections (14 µm) which were collected onto Superfrost Plus™ microscope slides (Menzel-Gläser, Braunschweig, Germany); sections were stored at –80°C until use.

Immunohistochemistry

Sections were air-dried, rehydrated in PBS, followed by 0.2% Triton X-100 and 5% normal donkey serum in PBS. The sections were incubated with primary antibody in 0.2% Triton X-100 and 5% normal donkey serum in PBS, overnight at 4°C. The following primary antibodies were used for cellular quantification: IBA1 for resident microglia (goat, 1:500, Abcam, Melbourne, Victoria, Australia); ED1 for activated microglia/macrophages (mouse, 1:500, Merck Millipore, Bayswater, Victoria, Australia); Olig2 (goat, 1:250, R&D Systems Inc., Minneapolis, MN, USA) together with NG2 (mouse, 1:500, Merck Millipore) for oligodendrocyte precursor cells (OPCs). Axonal integrity and myelin were assessed using antibodies recognizing: βIII-tubulin for optic nerve axons (mouse, 1:1,000, Covance, North Ryde, NSW, Australia); a commonly phosphorylated form of Tau at serine 396 (rabbit, pTau s396, 1:400, Life Technologies, Mulgrave, VIC, Australia) and pan Tau (mouse, 1:400, Life Technologies) for microtubule stability; myelin basic protein (MBP; goat, 1:500, Merck Millipore) for myelinated axons; and Caspr for paranodes within nodes of Ranvier (rabbit, 1:500, Abcam). Oxidative stress was assessed using antibodies recognizing 3-nitrotyrosine (3NT) for protein nitration (mouse, 1:500, Abcam), manganese superoxide dismutase (MnSOD) for antioxidant capacity (rabbit, 1:500, Enzo Life Sciences, Farmingdale, New York, USA), and 4-hydroxynonenal (HNE, rabbit 1:500, Alpha Diagnostics, San Antonio, Texas, USA) and acrolein (rabbit, 1:500, Abcam) for lipid peroxidation.

The following day sections were washed three times in PBS, and incubated with fluorophore-conjugated species-specific secondary antibodies (1:400, Alexa Fluor 488, 555, 647, Molecular Probes) and Hoechst nuclear stain (0.5 µL/mL, Invitrogen, Scoresby, Victoria, Australia) at room temperature for 2 hours. Sections were washed in PBS and cover-slipped in Fluoromount G (Southern Biotechnology, Birmingham, Alabama, USA). All sections for each antibody combination were immunostained at the same time to ensure uniformity of immunohistochemical procedures.

Imaging and analysis

Imaging for semi-quantification was performed using a Nikon, TI-E Inverted Microscope, controlled by NIS elements version 4.0 software (images deconvolved using NIS software), or a confocal Nikon c2 mounted on an upright Ni-E microscope, controlled by NIS elements 4.3 software (Nikon Australia, Rhodes, NSW, Australia). A single image was taken from a single section from each animal, of the optic nerve region directly ventral to the primary PT if present. This ventral region of the optic nerve is exclusively vulnerable to secondary degeneration (Fitzgerald et al., 2009a) and was used for all analyses of the current study. Images were edited and analyzed with ImageJ (FIJI version 1.5e, Schindelin et al., 2012), ensuring precise consistency of adjustments for images from all animals for any given analysis.

Cell counts for microglia/ macrophages and OPCs and immunointensity analyses for MBP, β-III tubulin, Tau and oxidative stress measures were conducted in accordance with previously published procedures (Payne et al., 2013; Szymanski et al., 2013; O'Hare Doig et al., 2014). Intensity analyses were performed on the single most in focus visual slice within each image, using ImageJ/Fiji analysis software (Schindelin et al., 2012) to semi-quantify the mean intensity or area of fluorescence; area based assessments were normalized for the area analyzed.

Analyses of the structure of the node of Ranvier and associated paranodes were conducted using our previously published techniques (Savigni et al., 2013; Szymanski et al., 2013). In brief, the optic nerve was imaged ventral to the injury at 40× optical magnification to detect immunoreactivity of βIII-tubulin and Caspr in 6 µm z-stacks at 0.5 µm optical thickness. For stereological analysis, a grid was overlayed with square box area equal to 1,250 μm^2; the labelled node/paranode structure closest to the upper-left corner in each grid square was quantified. 21 to 45 complexes were analyzed per animal, assessing mean length of the two paranodes in a complex, the length of the paranodal gap, and the length of the total complex, manually scrolling up and down the z-plane to ensure the full length of each feature was present and in focus within the z-stack.

Statistical analysis

Unless stated otherwise, all statistical testing was performed using one-way analysis of variance (ANOVA) and met the required assumptions. If the ANOVA was significant, Dunnett's *post-hoc* tests were used, with the PT-Veh group serving as the control comparison. For selected comparisons, Student's *t*-tests were used or Spearman's rank correlation analyses performed. An $\alpha = 0.05$ threshold was used for testing of significance. All statistical analyses were performed using the statistical program R (version 3.2.2, R Foundation for Statistical Computing, Vienna, Austria) in R Studio (version 0.99.482, RStudio Inc., Boston, MA, USA) with packages ez (version 4.2-2, M.A. Lawrence), multcomp (version 1.4-5, Hothorn et al., 2008) and plyr (version 1.8.3, Wickham, 2011). ANOVA results are presented in the form $F(df_{Group}, df_{Sample}) = F$-statistic, P-value), and for *post-hoc* tests

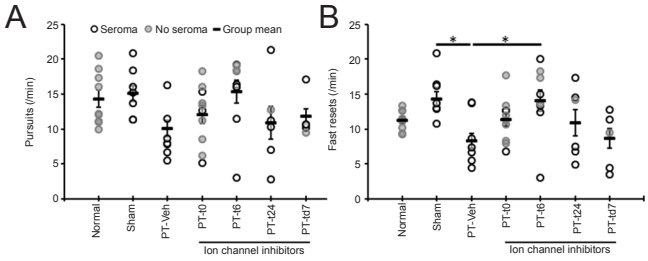

Figure 1 The effects of partial optic nerve transection (PT) and immediate or delayed ion channel inhibitor treatment on visual function.
Mean and distribution of responses per minute in the optokinetic nystagmus test of visual function; pursuits (A) and fast resets (B). Significant differences compared to PT-Veh determined by one-way analysis of variance followed by Dunnett's *post-hoc* test are indicated by $*P < 0.05$. N = 6–11 per group (see Table 1 for details). Normal, sham, PT-Veh, PT-t0, PT-t6, PT-t24 and PT-td7 indicate the groups as described in Table 1.

only the *P*-value is indicated.

Results

General observations: presence of seromas

Following surgery, seromas developed at the pump location in a significant number of the surgical intervention groups (**Table 1**), perhaps due to the large size of the pumps relative to the small PVG rats, and regardless of aseptic surgical practices incorporating enhanced sterility. Note that seromas have not been observed in our previous studies involving PT surgery (Fitzgerald et al., 2009b, 2010; O'Hare Doig et al., 2014), and were small and rarely observed when using the Alzet mini-osmotic pumps (Savigni et al., 2013). Animal ethics protocol restrictions precluded use of antibiotics. Seromas were periodically drained of fluid as required for animal welfare. Animals were monitored by a veterinarian and did not appear to be systemically ill. There is no indication that bacteria or

Table 1 Summary of incidence of seromas in Piebald Virol Glaxo rats for each experimental group

	Normal	Sham	PT-Veh	PT-t0	PT-t6	PT-t24	PT-td7
No seroma (*n*)	11	0	0	7	2	1	1
Seroma (*n*)	0	10	9	3	4	5	5
Total (*n*)	11	10	9	10	6	6	6
Seroma (%)	0	100	100	30	67	83	83

N = number of animals. Normal, sham, PT-Veh, PT-t0, PT-t6, PT-t24 and PT-td7 indicate groups respectively receiving no surgery; surgical preparation for the partial optic nerve transection (PT) surgery and pump implantation with immediate delivery of vehicle (Veh), but no cut of the dura surrounding the optic nerve and PT surgery; PT and pump implantation, with immediate delivery of Veh; PT and pump implantation, with immediate delivery of Ca^{2+} channel inhibitors, or delayed delivery, with Ca^{2+} channel inhibitor treatment initiated at 6 hours, 24 hours or 7 days.

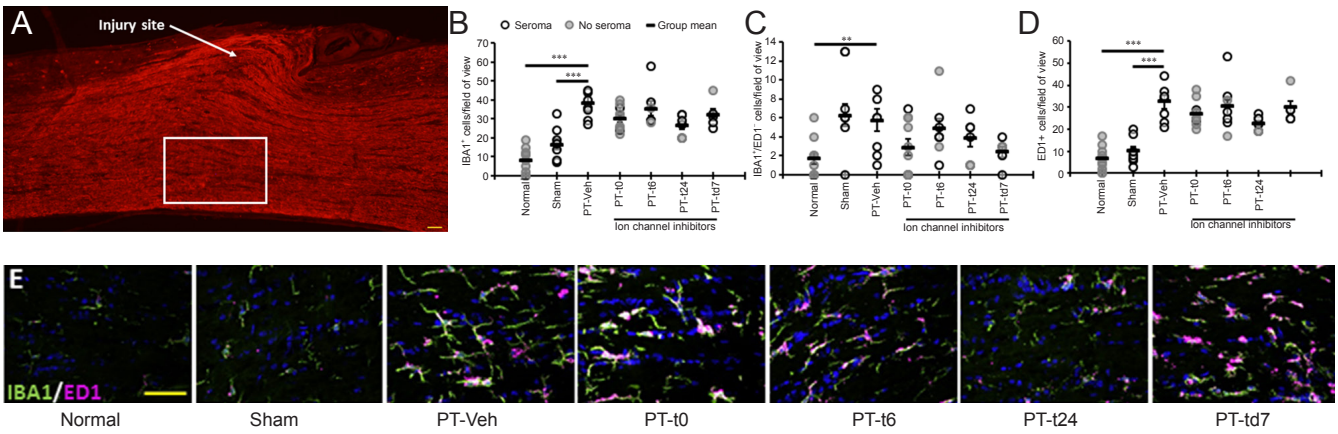

Figure 2 The effects of partial optic nerve transection (PT) and immediate or delayed ion channel inhibitor treatment on resident microglia (IBA1) and macrophages (ED1) in ventral optic nerve vulnerable to secondary degeneration.
(A) A representative image of the PT injury site and the region of ventral optic nerve used for analyses (boxed), immunohistochemically labelled with β-III tubulin$^+$ axons (red). The mean and distribution of cell counts in a field of view (B) all microglia cells (IBA1$^+$; green), (C) microglia that are not activated (IBA1$^+$/ ED1$^-$), and (D) activated microglia/macrophages (ED1$^+$; purple). (E) Representative images of the IBA1 and ED1 labelling in the ventral optic nerve from each group. $**P < 0.01$, $***P < 0.001$ (one-way analysis of variance followed by Dunnett's *post-hoc* test). N = 6 – 11 per group (see Table 1 for details). Scale bars are 50 μm in A and E. Cell nuclei are labelled with Hoechst in blue. Normal, sham, PT-Veh, PT-t0, PT-t6, PT-t24 and PT-td7 indicate the groups as described in Table 1.

exudate made its way to the optic nerve injury site or affected the function of the pump. Pathology analysis of selected seroma samples taken by the veterinarian indicated the presence of Staphylococcus aureus. Student's *t*-tests were employed to compare outcomes +/– seroma for each treatment group and outcome measure where feasible, and no statistically significant differences or trends were found (all $P > 0.05$), although the small numbers of animals when groups were divided into +/– seroma reduced statistical power. Therefore, all animals within each group were pooled for statistical analyses, and data are presented using different symbols for animals with and without seroma, to ensure maximum clarity. It is worth

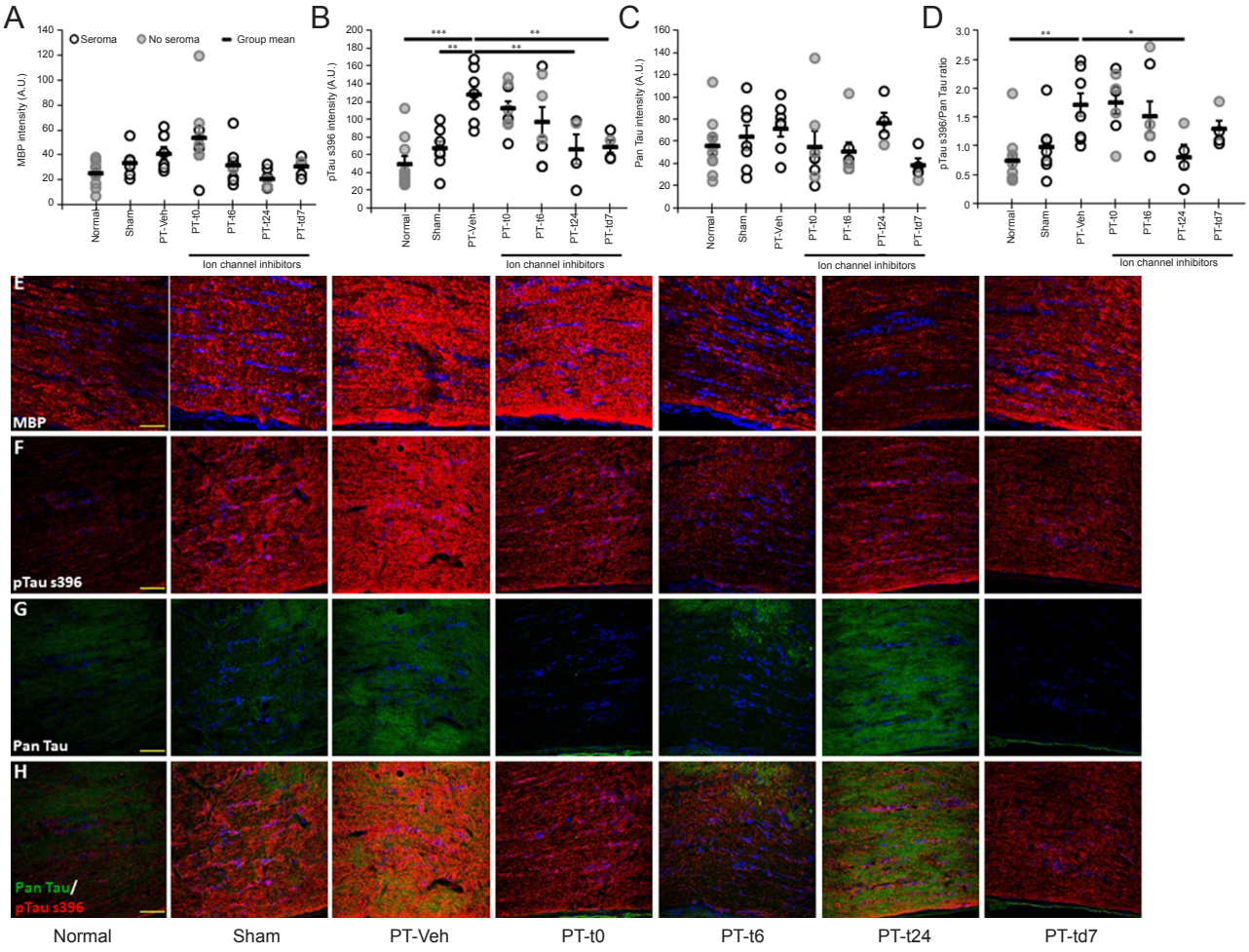

Figure 3 The effects of PT and immediate or delayed ion channel inhibitor treatment on immunoreactivity for markers of axonal and myelin structure in ventral optic nerve vulnerable to secondary degeneration.

(A–C) Mean and distribution of immunoreactivity in the ventral optic nerve shown for (A) myelin basic protein (MBP), (B) pTau s396. (C) pan Tau, (D) the ratio of pTau s396/pan Tau immunointensity in pan Tau-positive regions. (E–H) Representative images are shown for MBP (red) (E), pTau s396 (red) (F), pan Tau (green) (G), and composite images of pan Tau and pTau s396 (H). *$P < 0.05$, **$P < 0.01$, ***$P < 0.001$ (one-way analysis of variance followed by Dunnett's *post-hoc* test). N = 6–11 per group (see Table 1 for details). Scale bars: 50 μm, cell nuclei are labelled with Hoechst in blue. Normal, sham, PT-Veh, PT-t0, PT-t6, PT-t24 and PT-td7 indicate the groups as described in Table 1.

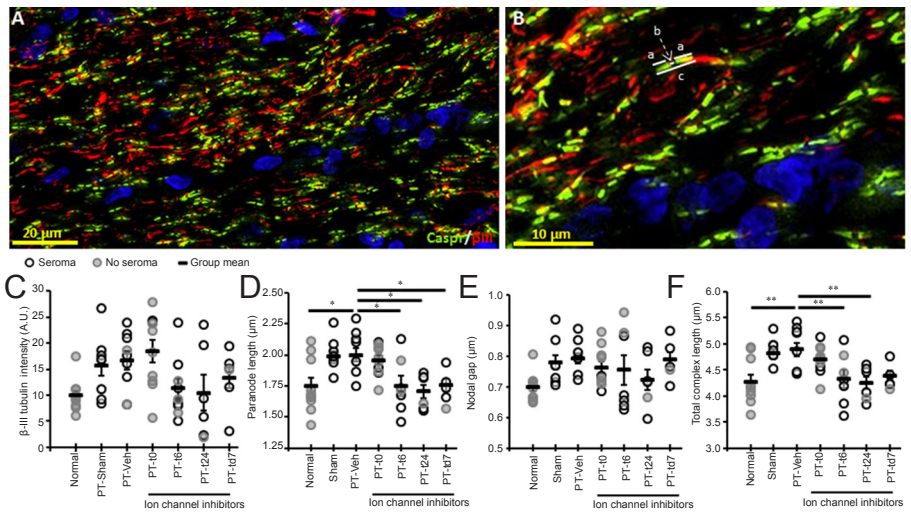

Figure 4 The effects of partial optic nerve transection (PT) and immediate or delayed ion channel inhibitor treatment on structure of the node of Ranvier in ventral optic nerve vulnerable to secondary degeneration.

(A) A representative image of the ventral optic nerve from a normal animal showing β-III tubulin-labelled axons (red) and paranode structure with Caspr (green). (B) Magnified view of (A) showing the elements of node/paranode structure that were quantified: lines indicated by 'a' are the paranode length; 'b' indicates the paranodal gap; and 'c' shows the total length of the node/paranode complex. Mean and distribution of immunoreactivity in the ventral optic nerve shown for (C) β-III tubulin immunoreactivity, (D) averaged length of both paranodes, (E) paranodal gap, and (F) total node/paranode complex length. *$P < 0.05$, **$P < 0.01$ (one-way analysis of variance followed by Dunnett's *post-hoc* test). N = 6–11 per group (see Table 1 for details). For (A) and (B) scale bars are 20 μm and 10 μm respectively. Cell nuclei are labelled with Hoechst in blue. Normal, sham, PT-Veh, PT-t0, PT-t6, PT-t24 and PT-td7 indicate the groups as described in Table 1.

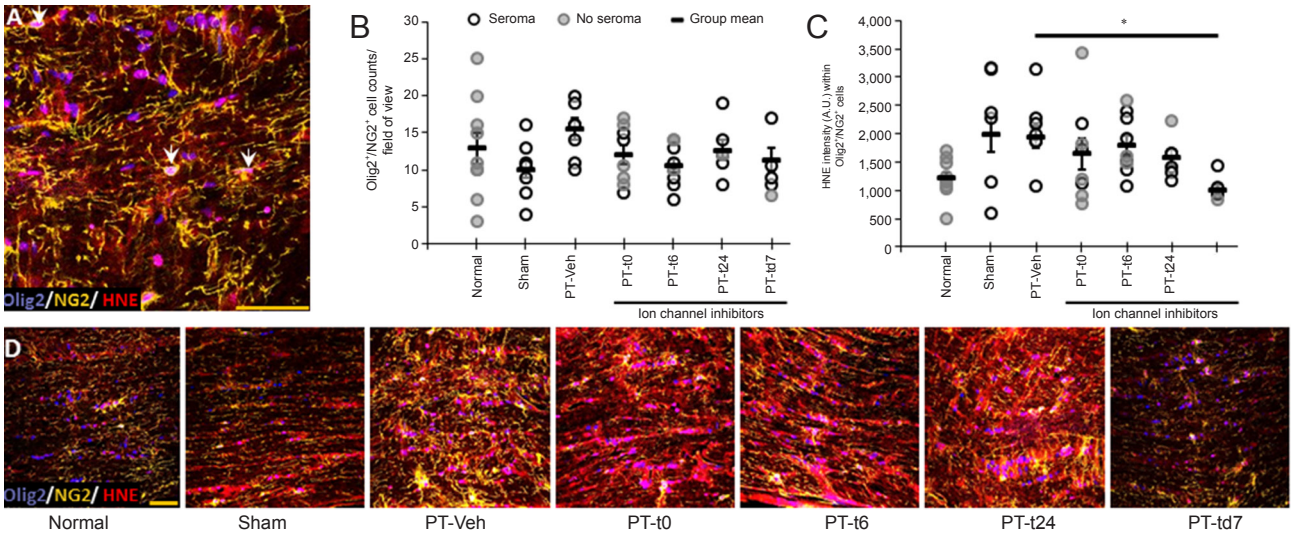

Figure 5 The effects of partial optic nerve transection (PT) and immediate or delayed ion channel inhibitor treatment on lipid peroxidation in oligodendrocyte precursor cells (OPCs) in ventral optic nerve vulnerable to secondary degeneration.
(A) A representative image of the co-localisation (white arrows) of Olig2 (purple) and NG2 (yellow), indicating OPCs, and 4-hydroxynonenal (HNE) immunofluorescence (red). (B) Mean and distribution of OPC numbers in a field of view from the ventral optic nerve. (C) Mean and distribution of immunoreactivity of HNE in $Olig2^{+}/NG2^{+}$ cells. (D) Representative images of Olig2 (purple), NG2 (yellow), and HNE (red) staining in the ventral optic nerve from animals from each experimental group. $^{*}P < 0.05$ (one-way analysis of variance followed by Dunnett's *post-hoc* test). N = 6–11 per group (see Table 1 for details). Scale bars: 50 μm, cell nuclei are labelled with Hoechst in blue. Normal, sham, PT-Veh, PT-t0, PT-t6, PT-t24 and PT-td7 indicate the groups as described in Table 1.

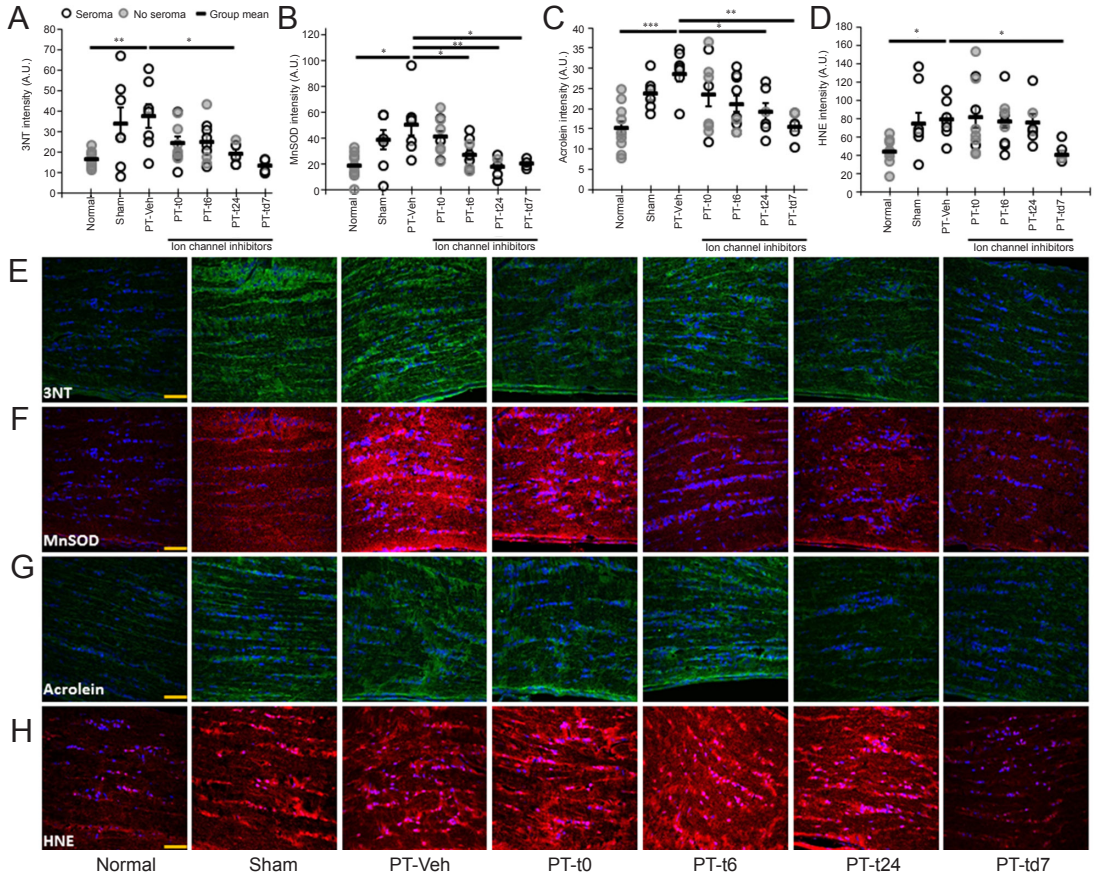

Figure 6 The effects of partial optic nerve transection (PT) and immediate or delayed ion channel inhibitor treatment on immunoreactivity of oxidative stress indicators in ventral optic nerve vulnerable to secondary degeneration.
(A–D) Immunointensity analysis showing the mean and distribution of intensity for (A) 3-nitrotyrosine (3NT) (green), (B) manganese superoxide dismutase (MnSOD) (red), (C) acrolein (green), and (D) 4-hydroxynonenal (HNE) (red). Representative images from each oxidative stress indicator are shown in (E) to (H) respectively. $^{*}P < 0.05$, $^{**}P < 0.01$, $^{***}P < 0.001$ (one-way analysis of variance followed by Dunnett's *post-hoc* test). N = 6–11 per group (see Table 1 for details). Scale bars: 50 μm, cell nuclei are labelled with Hoechst in blue. Normal, sham, PT-Veh, PT-t0, PT-t6, PT-t24 and PT-td7 indicate the groups as described in Table 1.

noting that all sham animals presented with seromas, as did all injured, vehicle treated animals (PT-Veh). In contrast, no animals treated immediately with the ion channel inhibitors developed seromas. Increasing delay of treatment initiation was associated with increasing incidence of seromas (**Table 1**). Spearman's rank correlation analysis indicated a significant correlation between seroma incidence and treatment delay (R = 0.558, S = 3,723.9, P value = 0.0003), although it is important to note that group numbers are small and results should be interpreted with caution.

Visual function

Two weeks after PT, all rats were assessed for optokinetic nystagmus pursuit and fast reset responses as an indication of visual function (**Figure 1**). There was no significant difference in the total number of pursuits between groups ($F_{(6, 53)}$ = 1.588, P = 0.17). However, there was a significant difference in the number of fast resets per minute ($F_{(6, 53)}$ = 2.734, P < 0.05). Post-hoc comparisons revealed that there were fewer resets in the PT-Veh group compared to both the sham (P < 0.05) and PT-t6 (P < 0.05) groups, indicating both the expected reduction in number of responses with injury (Fitzgerald et al., 2009b), and a beneficial effect of treatment delayed for 6 hours after injury.

Microglia/ macrophage cell numbers

Cellular and structural outcomes were assessed in optic nerve ventral to the PT injury site (**Figure 2A**). The effects of sham surgery or PT with vehicle or ion channel inhibitors on microglia/macrophage numbers in the ventral optic nerve, were assessed using IBA1 as a marker of resident microglia, and/or ED1 as an indicator of activated microglia/macrophages (**Figure 2B**–**E**). As expected and in line with our previous work (Fitzgerald et al., 2009b), ANOVA revealed significant differences in the numbers of resident IBA1$^+$ cells between experimental groups ($F_{(6, 55)}$ = 12.65, P < 0.001), with post-hoc tests indicating that PT–Veh had more microglia compared to both the normal (P < 0.001) and sham groups (P < 0.001; **Figure 2B**). However, there were no differences between vehicle and ion channel inhibitor treatment groups (P > 0.05; **Figure 2B**). Similarly, there were also changes in the number of resident resting microglia between experimental groups (IBA1$^+$/ED1$^-$, $F_{(6, 55)}$ = 3.102, P < 0.05; **Figure 2C**), with increased numbers of resting microglia in PT-Veh compared to the normal group (P < 0.01), although numbers of resting microglia in PT-Veh were not different from sham group (P > 0.05). There were no differences between PT-Veh and any of the ion channel inhibitor treated groups (all P > 0.05). The total numbers of activated ED1$^+$ microglia/macrophages were also different in the various experimental groups ($F_{(6, 55)}$ = 14.9, P < 0.0001; **Figure 2D**). *Post-hoc* tests revealed that PT-Veh had elevated numbers of ED1$^+$ cells compared to both normal (P < 0.001) and sham (P < 0.001) groups. Once again, there were no effects of Ca^{2+} channel inhibitor treatment, relative to PT-Veh (all P > 0.05). Note that all ED1$^+$ cells were also IBA1$^+$. There were no indications that seromas over the drug delivery pump on the flank of the animal affected the numbers of microglia/macrophages in the optic nerve, as overlap between data points from animals with or without seromas was evident (**Figure 2B**–**D**).

Components of myelin and axons

MBP immunofluorescence, assessed in ventral optic nerve as an indicator of myelin integrity, was significantly different between groups ($F_{(6, 47)}$ = 3.475, $P \leq 0.01$; **Figure 3A**). However, *post-hoc* analysis did not reveal significant differences between PT-Veh and other experimental groups (P > 0.05). The immunointensity of the microtubule-associated protein pTau s396 was also different between experimental groups ($F_{(6, 46)}$ = 7.308, P < 0.0001; **Figure 3B**). Specifically, *post-hoc* analysis revealed that pTau s396 immunoreactivity was greater in the injury group PT-Veh compared to the uninjured groups, normal (P < 0.001) and sham (P < 0.01). In addition, ion channel inhibitor treatment delayed by 24 hours (PT-t24, P < 0.01) or 7 days (PT-td7, P < 0.01) resulted in reduced immunofluorescence of pTau s396, relative to PT-Veh. The immunointensity of pan Tau was not significantly different between experimental groups ($F_{(6, 46)}$ = 1.446, P = 0.22; **Figure 3C**). When analyses were confined to pan Tau immunopositive regions, calculation of the ratio of pTau s396/pan Tau immunointensity revealed significant differences ($F_{(6, 46)}$ = 4.149, $P \leq 0.01$; **Figure 3D**). Specifically, the ratio was elevated for PT-Veh compared to normal ($P \leq 0.01$), and delaying ion channel inhibitor treatment by 24 hours reduced the ratio of pTau s396 /pan Tau (PT-t24, P < 0.05). β-III tubulin immunofluorescence, assessed in ventral optic nerve as an indicator of axonal integrity, was significantly different between groups ($F_{(6, 49)}$ = 2.791, P = 0.0205; **Figure 4C**). However, post-hoc analysis did not reveal significant differences between PT-Veh and other experimental groups (P > 0.05). Once again, seromas did not appear to have any consistent effect on indicators of myelin or axonal structure within each group (**Figure 3A**–**D**).

Structure of the node of Ranvier

The structure of the node of Ranvier in ventral optic nerve susceptible to secondary degeneration was assessed using Caspr and βIII-tubulin immunoreactivity to delineate paranodes and the paranodal gap, indicative of the length of the node, respectively (**Figure 4A**, **B**). The paranode length was affected by experimental treatments ($F_{(6, 54)}$ = 4.948, $P \leq 0.001$; **Figure 4D**). In line with our previously published outcomes (Szymanski et al., 2013), the PT-Veh group exhibited paranode lengthening compared to normal group. Ion channel inhibitor treatment delayed by 6 or 24 hours or 7 days after injury resulted in significant reductions in paranode length (all P < 0.05). However, there was no difference between PT-Veh and sham groups (P > 0.05), and immediate treatment did not result in any change to paranode length relative to PT-Veh control (P > 0.05; **Figure 4D**). The paranodal gap was not different between experimental groups at this timepoint after injury ($F_{(6, 54)}$ = 1.839, P = 0.109; **Figure 4E**). The total length of the node/paranode complex was different between experimental groups ($F_{(6, 54)}$ = 4.881, P < 0.001; **Figure**

4F). Significant lengthening of the complex was observed as a consequence of PT injury, and ion channel inhibitor treatment delayed by 6 or 24 hours led to significant reductions relative to PT-Veh (all $P < 0.01$; **Figure 4F**). Seromas did not have any consistent effect on node/paranode structure within each group (**Figure 4C–F**).

Oxidative stress in OPCs

The number of OPCs and the degree of lipid peroxidation within these cells were examined in ventral optic nerve (**Figure 5**). The total number of OPCs was unchanged between experimental groups ($F_{(6, 56)} = 1.541$, $P = 0.182$; **Figure 5B**). This finding is in contrast to our previous report of depleted OPCs following PT injury (Payne et al., 2013), and may have occurred as a consequence of seromas in the PT-Veh group. However, lipid peroxidation, indicated by HNE immunofluorescence, was changed within OPCs as a consequence of experimental treatment ($F_{(6, 51)} = 2.561$, $P < 0.05$; **Figure 5C**). Specifically, HNE intensity within OPCs was significantly reduced with ion channel inhibitor treatment when treatment was delayed by 7 days, compared to PT-Veh (PT-td7, $P < 0.05$). There were no other significant changes relative to PT-Veh, including sham (all $P > 0.05$). Seromas did not consistently influence either OPC numbers, or HNE intensity in OPCs within each group (**Figure 5B**, **C**).

Oxidative stress throughout the vulnerable optic nerve

The effects of sham or PT injury and vehicle or inhibitor treatment on the oxidative stress indicators 3NT, MnSOD, acrolein, and HNE were assessed in ventral optic nerve vulnerable to secondary degeneration. Protein nitration indicated by 3NT immunoreactivity was significantly different between experimental groups ($FF_{(6, 43)} = 3.43$, $P \leq 0.01$; **Figure 6A**, **E**). 3NT immunoreactivity was elevated in PT-Veh group relative to normal group ($P < 0.01$) and delayingion channel inhibitor treatment by 24 hours led to a significant reduction (PT-t24, $P < 0.05$). There were no differences between the PT-Veh group and other treatment groups, including sham (all $P > 0.05$). There was also a change in immunointensity of the antioxidant enzyme MnSOD between experimental groups ($F_{(6, 43)} = 4.51$, $P < 0.01$; **Figure 6B**, **F**), with PT-Veh group exhibiting significantly higher immunofluorescence than normal group ($P \leq 0.05$) and delayed treatment resulting in significant reductions in the PT-t6 ($P \leq 0.05$), PT-t24 ($P < 0.01$), and PT-td7 ($P \leq 0.05$) groups. However, there were no significant differences between PT-Veh and sham groups ($P > 0.05$), or following immediate treatment (PT-t0, $P > 0.05$). Indicators of lipid peroxidation, acrolein ($F(6, 47) = 4.62$, $P < 0.001$, **Figure 6C**, **G**) and HNE ($F_{(6, 51)} = 3.19$, $P \leq 0.01$; **Figure 6D**, **H**) also differed between groups.

Acrolein immunointensity was significantly greater in the PT–Veh group than in the normal group ($P \leq 0.001$), but there was no significant difference between PT-Veh and sham groups ($P > 0.05$). Acrolein immunointensity was significantly decreased after treatment delayed by 24 hours or 7 days compared to PT-Veh (PT-t24, $P \leq 0.05$; PT-td7, $P < 0.01$). Similarly, HNE immunointensity was significantly increased in the PT-Veh group than in the normal group ($P < 0.05$), but there was no significance between PT-Veh and sham groups ($P > 0.05$). HNE immunointensity was only decreased by ion channel inhibitor treatment delayed by 7 days (PT-td7, $P < 0.05$). There were no consistent effects of seromas on any of oxidative stress indicators that were assessed (**Figure 6A–D**).

Discussion

The purpose of this study was to examine how long one could delay treatment of secondary degeneration with a combination of ion channel inhibitors proven to provide long term benefits, and maintain efficacy. It is important to investigate the therapeutic window of treatment strategies, as intervention after neurotrauma such as spinal cord injury is rarely immediate, and treatment delays affect outcomes (Bracken et al., 1997). However, our study was confounded by the presence of seromas surrounding the programmable iPRECIO® treatment delivery pumps on the flanks of animals, indicating inadvertent infection following infusion-pump implantation. It is important to note that seromas or infections at the PT injury site have not been observed in this or our previous studies conducting PT injury (Fitzgerald et al., 2009b; Szymanski et al., 2013; O'Hare Doig et al., 2014); seromas surrounding implanted Alzet osmotic mini-pumps were small and extremely rare (Savigni et al., 2013).

Partial transection of the optic nerve resulted in acute deficits that were predominantly expected and in line with our reported outcomes (Fitzgerald et al., 2009b; Szymanski et al., 2013; O'Hare Doig et al., 2014), with reduced visual-motor responses, increased microglia/macrophage numbers, altered axonal stability and myelin structure and increases in indicators of oxidative stress. As previously described (Fitzgerald et al., 2010), the observed increases in myelin immunoreactivity with injury are likely due to altered myelin structure resulting in increased immunogenicity, rather than any increases in myelin. Increased MBP immunoreactivity has been shown to reflect a release of MBP into the surrounding milieu, accompanied by upregulated expression of MBP mRNA and protein (Bartholdi and Schwab, 1998), and/or conformational changes (Kozlowski et al., 2008). However, sham injured groups were sometimes not different from PT injured and vehicle treated animals, particularly for indicators of node/paranode structure and oxidative stress. This is in contrast to our previous reports of no effect of sham PT surgery relative to normal (Fitzgerald et al., 2009b). Furthermore, the response of OPCs to secondary degeneration was unexpected and not in line with our previous reports (Payne et al., 2013), with no reduction in OPC numbers with PT injury. Current and ongoing parallel studies in our laboratory have confirmed our reported depletion of OPC numbers with PT injury (manuscript in preparation), indicating that the presence of seromas in PT vehicle treated animals has impacted upon the normal depletion of OPC numbers, countering the expected decrease with PT injury.

Aspects of secondary degeneration were responsive to

treatment with the combination of ion channel inhibitors. The combinatorial treatment strategy preserved visual function, limited disruptions to axonal integrity and node/paranode structure, and reduced oxidative stress, consistent with improvements reported in our previous studies (Fitzgerald et al., 2009b; Savigni et al., 2013). However, the expected simple correlation of increasing efficacy with speed of initiation of treatment was not observed. For example, oxidative stress was reduced most effectively when treatment was delayed by 7 days. Indeed, immediate treatment did not result in any significant improvements in the indices assessed in this study. This is in direct contrast to our reported beneficial effects on function, myelin compaction and node/paranode structure, when outcomes of 2 weeks of oxATP and YM872 treatment, together with continuous lomerizine treatment, were assessed at 3 months following injury (Savigni et al., 2013). It is possible that at 2 weeks after injury, the combination of ion channel inhibitors does not result in beneficial effects when treatment is initiated at the time of injury, indicating some form of transient lack of efficacy that is rescued by maintaining lomerizine treatment until 3 months after injury. However, we consider it perhaps more likely that the presence of seromas has confounded outcomes and may have led to competing interactions with the ion channel inhibitors. There is no clear clustering of data points +/- seroma for any of the outcome measures assessed, however subtle skewing of outcomes is possible. Indeed, the lack of any seromas in animals where treatment was initiated at the time of PT surgery and pump implantation indicates that the ion channel inhibitors may have in some way limited seroma formation, and in so doing reduced bioavailability of the inhibitors to counter the spread of secondary degeneration. Such an effect is more likely for lomerizine, which was orally administered and therefore more systemically bioavailable than oxATP and YM872 delivered directly to the optic nerve injury site. Search of the literature did not reveal reports of direct anti-bacterial or anti-seroma effects of ion channel inhibitors. While application of the Ca^{2+} channel inhibitors verapamil, nifedipine and diltiazem inhibit the *in vitro* destruction of *Staphylococcus Aureus* by monocytes and peritoneal polymorphonuclear cells (Levy et al., 1991), our observation of no seromas in animals where treatment was initiated at the time of PT surgery and pump implantation argues against such an effect in this particular scenario. Anti-inflammatory effects of Ca^{2+} channel inhibitors have been reported *in vivo* and a similar mechanism may be operating here (Huang et al., 2014).

The bacterium detected in the seromas was *Staphylococcus aureus*, which expresses a variety of neurodegenerative factors, such as lipoteichoic acid (LTA) and α-toxin. *In vivo* application of LTA to cell cultures results in neuronal death, which is likely mediated by activation of microglia and astrocytes, resulting in oxidative and nitrosative stress (Kinsner et al., 2005; Boveri et al., 2006). In addition, LTA disrupts the blood-brain barrier, resulting in the release of inflammatory cytokines (Boveri et al., 2006; Sheen et al., 2010), further inducing vulnerability in the central nervous system. α-Toxin is extravasated during blood-brain barrier breach (Sjogren et al., 1991), binds directly to nerves (Szmigielski and Harshman, 1978) and damages myelin (Harshman et al., 1985) *via* excess phosphorylation of MBP (Chan and Lazarovici, 1987), resulting in myelin destabilization (Boggs, 2006). As such, α-toxin may have contributed to degeneration of axons and myelin in animals in which seromas were observed, for example, increasing indicators of secondary degeneration in sham injured animals. *Staphylococcus* toxins LTA and α-toxin utilize pathways that mediate damage which are Ca^{2+}-channel independent (Suttorp et al., 1985; Bantel et al., 2001; Ginsburg, 2002), and are therefore unlikely to be affected by the combination of ion channel inhibitors used in the current study. Nevertheless, we observed beneficial effects of the combination of ion channel inhibitors in the presence of seromas when treatment was delayed, indicating that the inhibitors were effective in this context, in spite of concomitant infection.

Conclusion

The current study demonstrates that peripheral infection may confound outcomes of ion channel inhibitor treatments, masking both assessments of pathology of secondary degeneration and the treatment response. This highlights the need for careful control of infection and use of prophylactic antibiotics in both clinical populations and animal studies, as the benefits of therapies may only be apparent in aseptic environments. Despite this, beneficial functional, structural and metabolic effects of the combination of the ion channel inhibitors lomerizine, oxATP and YM872 were observed, even when treatment was delayed for as long as 7 days after injury. Our data support the clinical utility of this combinatorial inhibitor approach.

Author contributions: *Study conception: MF; study design: MF and CAB; experiment conduction: NJY, MKG, RLO'HD, WC, BEA, JK, CAB, MF; data acquisition: NJY, MKG, CAB; data analysis: NJY, MKG, MF; statistical analysis: NJY, MKG and MF; manuscript preparation: NJY, WC, MKG, CAB and MF; manuscript editing and manuscript review: NJY, MKG, RLO'HD, WC, CAB and MF.*
Conflicts of interest: *None declared.*
Plagiarism check: *This paper was screened twice using CrossCheck to verify originality before publication.*
Peer review: *This paper was double-blinded and stringently reviewed by international expert reviewers.*

References

Abdeljalil J, Hamid M, Abdel-Mouttalib O, Stéphane R, Raymond R, Johan A, José S, Pierre C, Serge P (2005) The optomotor response: a robust first-line visual screening method for mice. Vision Res 45:1439-1446.

Agrawal SK, Nashmi R, Fehlings MG (2000) Role of L- and N-type calcium channels in the pathophysiology of traumatic spinal cord white matter injury. Neuroscience 99:179-188.

Akaike N, Ishibashi H, Hara H, Oyama Y, Ueha T (1993) Effect of KB-2796, a new diphenylpiperazine Ca2+ antagonist, on voltage-dependent Ca2+ currents and oxidative metabolism in dissociated mammalian CNS neurons. Brain Res 619:263-270.

Bantel H, Sinha B, Domschke W, Peters G, Schulze-Osthoff K, Jänicke RU (2001) α-Toxin is a mediator of Staphylococcus aureus–induced cell death and activates caspases via the intrinsic death pathway independently of death receptor signaling. J Cell Biol 155:637-648.

Bartholdi D, Schwab ME (1998) Oligodendroglial reaction following spinal cord injury in rat: transient upregulation of MBP mRNA. Glia 23:278-284.

Boggs JM (2006) Myelin basic protein: a multifunctional protein. Cell Mol Life Sci 63:1945-1961.
Boveri M, Kinsner A, Berezowski V, Lenfant AM, Draing C, Cecchelli R, Dehouck MP, Hartung T, Prieto P, Bal-Price A (2006) Highly purified lipoteichoic acid from gram-positive bacteria induces in vitro blood–brain barrier disruption through glia activation: Role of pro-inflammatory cytokines and nitric oxide. Neuroscience 137:1193-1209.
Bracken MB, Shepard M, Holford TR, et al. (1997) Administration of methylprednisolone for 24 or 48 hours or tirilazad mesylate for 48 hours in the treatment of acute spinal cord injury: Results of the third national acute spinal cord injury randomized controlled trial. JAMA 277:1597-1604.
Camello-Almaraz MC, Pozo MJ, Murphy MP, Camello PJ (2006) Mitochondrial production of oxidants is necessary for physiological calcium oscillations. J Cell Physiol 206:487-494.
Chan KF, Lazarovici P (1987) Staphylococcus aureus α-toxin. 1. Effect on protein phosphorylation in myelin. Toxicon 25:631-636.
Fitzgerald M, Bartlett CA, Harvey AR, Dunlop SA (2010) Early events of secondary degeneration after partial optic nerve transection: an immunohistochemical study. J Neurotrauma 27:439-452.
Fitzgerald M, Payne SC, Bartlett CA, Evill L, Harvey AR, Dunlop SA (2009a) Secondary retinal ganglion cell death and the neuroprotective effects of the calcium channel blocker lomerizine. Invest Ophthalmol Vis Sci 50:5456-5462.
Fitzgerald M, Bartlett CA, Evill L, Rodger J, Harvey AR, Dunlop SA (2009b) Secondary degeneration of the optic nerve following partial transection: the benefits of lomerizine. Exp Neurol 216:219-230.
Ginsburg I (2002) Role of lipoteichoic acid in infection and inflammation. Lancet Infect Dis 2:171-179.
Hamilton N, Vayro S, Kirchhoff F, Verkhratsky A, Robbins J, Gorecki DC, Butt AM (2008) Mechanisms of ATP-and glutamate-mediated calcium signaling in white matter astrocytes. Glia 56:734-749.
Harshman S, Burt AM, Robinson JP, Blankenship M, Harshman DL (1985) Disruption of myelin sheaths in mouse brain in vitro and in vivo by staphylococcal α-toxin. Toxicon 23:801-806.
Hothorn T, Bretz F, Westfall P (2008) Simultaneous inference in general parametric models. Biom J 50:346-363.
Huang BR, Chang PC, Yeh WL, Lee CH, Tsai CF, Lin C, Lin HY, Liu YS, Wu CY, Ko PY, Huang SS, Hsu HC, Lu DY (2014) Anti-neuroinflammatory effects of the calcium channel blocker nicardipine on microglial cells: implications for neuroprotection. PLoS One 9:e91167.
Karim Z, Sawada A, Kawakami H, Yamamoto T, Taniguchi T (2006) A new calcium channel antagonist, lomerizine, alleviates secondary retinal ganglion cell death after optic nerve injury in the rat. Curr Eye Res 31:273-283.
Kinsner A, Pilotto V, Deininger S, Brown GC, Coecke S, Hartung T, Bal-Price A (2005) Inflammatory neurodegeneration induced by lipoteichoic acid from Staphylococcus aureus is mediated by glia activation, nitrosative and oxidative stress, and caspase activation. J Neurochem 95:1132-1143.
Korinek AM (1997) Risk factors for neurosurgical site infections after craniotomy: a prospective multicenter study of 2944 patients. The French Study Group of Neurosurgical Infections, the SEHP, and the C-CLIN Paris-Nord. Service Epidémiologie Hygiène et Prévention. Neurosurgery 41:1073-1081.
Kozlowski P, Raj D, Liu J, Lam C, Yung AC, Tetzlaff W (2008) Characterizing white matter damage in rat spinal cord with quantitative MRI and histology. J Neurotrauma 25:653-676.
Levkovitch-Verbin H, Quigley HA, Martin KR, Zack DJ, Pease ME, Valenta DF (2003) A model to study differences between primary and secondary degeneration of retinal ganglion cells in rats by partial optic nerve transection. Invest Ophthalmol Vis Sci 44:3388-3393.
Levy R, Dana R, Gold B, Alkan M, Schlaeffer F (1991) Influence of calcium channel blockers on polymorphonuclear and monocyte bactericidal and fungicidal activity. Isr J Med Sci 27:301-306.
Matute C, Torre I, Pérez-Cerdá F, Pérez-Samartín A, Alberdi E, Etxebarria E, Arranz AM, Ravid R, Rodríguez-Antigüedad A, Sánchez-Gómez M (2007) P2X7 receptor blockade prevents ATP excitotoxicity in oligodendrocytes and ameliorates experimental autoimmune encephalomyelitis. J Neurosci 27:9525-9533.
Oconnor E, Venkatesh B, Mashongonyika C, Lipman J, Hall J, Thomas P (2004) Serum procalcitonin and C-reactive protein as markers of sepsis and outcome in patients with neurotrauma and subarachnoid haemorrhage. Anaesth Intensive Care 32:465-470.
O'Hare Doig RL, Fitzgerald M (2015) Novel combinations of ion channel inhibitors for treatment of neurotrauma. Discov Med 19:41-47.
O'Hare Doig RL, Bartlett CA, Maghzal GJ, Lam M, Archer M, Stocker R, Fitzgerald M (2014) Reactive species and oxidative stress in optic nerve vulnerable to secondary degeneration. Exp Neurol 261C:136-146.
Park E, Velumian AA, Fehlings MG (2004) The role of excitotoxicity in secondary mechanisms of spinal cord injury: a review with an emphasis on the implications for white matter degeneration. J Neurotrauma 21:754-774.
Payne SC, Bartlett CA, Savigni DL, Harvey AR, Dunlop SA, Fitzgerald M (2013) Early proliferation does not prevent the loss of oligodendrocyte progenitor cells during the chronic phase of secondary degeneration in a CNS white matter tract. PLoS One 8:e65710.
Peng TI, Jou MJ (2010) Oxidative stress caused by mitochondrial calcium overload. Ann N Y Acad Sci 1201:183-188.
Prusky GT, Harker KT, Douglas RM, Whishaw IQ (2002) Variation in visual acuity within pigmented, and between pigmented and albino rat strains. Behav Brain Res 136:339-348.
Savigni DL, O'Hare Doig RL, Szymanski CR, Bartlett CA, Lozic I, Smith NM, Fitzgerald M (2013) Three Ca channel inhibitors in combination limit chronic secondary degeneration following neurotrauma. Neuropharmacology 75C:380-390.
Schindelin J, Arganda-Carreras I, Frise E, Kaynig V, Longair M, Pietzsch T, Preibisch S, Rueden C, Saalfeld S, Schmid B, Tinevez JY, White DJ, Hartenstein V, Eliceiri K, Tomancak P, Cardona A (2012) Fiji: an open-source platform for biological-image analysis. Nat Methods 9:676-682.
Selt M, Bartlett CA, Harvey AR, Dunlop SA, Fitzgerald M (2010) Limited restoration of visual function after partial optic nerve injury; a time course study using the calcium channel blocker lomerizine. Brain Res Bull 81:467-471.
Sheen TR, Ebrahimi CM, Hiemstra IH, Barlow SB, Peschel A, Doran KS (2010) Penetration of the blood–brain barrier by Staphylococcus aureus: contribution of membrane-anchored lipoteichoic acid. J Mol Med (Berl) 88:633-639.
Sjogren AM, Thelestam M, Blomqvist L, Linda H, Remahl S, Risling M (1991) Extravasation of staphylococcal alpha-toxin in normal and injured CNS regions lacking blood-brain barrier function: observations after ventral root replantation. Brain Res 559:276-282.
Suttorp N, Seeger W, Dewein E, Bhakdi S, Roka L (1985) Staphylococcal alpha-toxin-induced PGI2 production in endothelial cells: role of calcium. Am J Physiol 248:C127-134.
Szmigielski S, Harshman S (1978) Specific binding of staphylococcal alpha-toxin to isolated rabbit vagus nerves in vitro. Infect Immun 21:1024-1026.
Szymanski CR, Chiha W, Morellini N, Cummins N, Bartlett CA, O'Hare Doig RL, Savigni DL, Payne SC, Harvey AR, Dunlop SA, Fitzgerald M (2013) Paranode abnormalities and oxidative stress in optic nerve vulnerable to secondary degeneration: modulation by 670 nm light treatment. PLoS One 8:e66448.
Wickham H (2011) The split-apply-combine strategy for data analysis. J Stat Softw 40:1-29.
Yoles E, Muller S, Schwartz M (1997) NMDA-receptor antagonist protects neurons from secondary degeneration after partial optic nerve crush. J Neurotrauma 14:665-675.

Copyedited by Li CH, Song LP, Zhao M